Journal of
Applied
Crystallography
ISSN 0021-8898

Received 10 February 2004
Accepted 25 May 2004

© 2004 International Union of Crystallography
Printed in Great Britain – all rights reserved

Interference phenomena observed by X-ray diffraction in nanocrystalline thin films

David Rafaja,[a]* Volker Klemm,[a] Gerhard Schreiber,[a] Michael Knapp[b] and Radomír Kužel[c]

[a]Institute of Physical Metallurgy, TU Bergakademie Freiberg, Gustav-Zeuner-Str. 5, D-09599 Freiberg, Germany, [b]Institute for Materials Science, TU Darmstadt, Petersenstr. 23, D-64287 Darmstadt, Germany, and [c]Department of Electronic Structures, Faculty of Mathematics and Physics, Charles University, CZ-121 16 Prague, Czech Republic. Correspondence e-mail: rafaja@ww.tu-freiberg.de

An increase of the X-ray diffraction line broadening with increasing diffraction angle was observed experimentally in nanocrystalline thin films. Such a change of the line width is usually related to the microstrain in the sample, which, however, contradicts the assumptions that the microstrain is relatively low in nanocrystalline materials and that the line broadening is caused mainly by small crystallite size. For nanocrystalline thin films, the observed changes in the diffraction line broadening are explained by a partial coherence of adjacent crystallites, which is stronger at low diffraction angles than at high diffraction angles. Furthermore, it is found that the degree of coherence of the adjacent crystallites depends on their size and preferred orientation. Smaller crystallites show better coherence, because the corresponding reciprocal-lattice points are broadened compared with those related to large crystallites. A strong preferred orientation improves further the coherence of the adjacent crystallites. Theoretical results are confirmed by experimental data obtained on nanocrystalline (Ti,Al)N thin films using a combination of glancing-angle X-ray diffraction, high-resolution transmission electron microscopy and X-ray texture analysis.

1. Introduction

X-ray diffraction is a powerful method for the investigation of the real structure of crystalline materials. From a powder diffraction pattern it is possible to extract information about crystallite size, strain, stress, texture and structural defects. Different approaches have been developed and applied to distinguish between different microstructural features. They are based either on a phenomenological or on a microstructural theory. Nevertheless, most of them utilize line profile analysis. The phenomenological approach works with a model of mosaic blocks containing microstrain; it is represented by the well known Warren theory (Warren, 1990). The microstructural approach is based on a model of a statistical distribution of specific lattice defects (first of all dislocations); it is represented by the Krivoglaz theory (Krivoglaz, 1996). Various modifications of both basic approaches have been developed in the past decade. A comprehensive review can be found in the books *Defect and Microstructure Analysis by Diffraction* (Snyder *et al.*, 1999) and *Diffraction Analysis of the Microstructure of Materials* (Mittemeijer & Scardi, 2003). The principle problem of the line broadening analysis is the separation of two effects that contribute to the diffraction line broadening: the lattice strain related to the lattice defects and the small size of crystallites. The line profile analysis can be performed either in a simplified way by using single profile parameters, namely the integral breadth (*i.e.* the integrated intensity of a diffraction profile divided by the peak height) and/or the full width at half-maximum (FWHM) (Williamson & Hall, 1953; de Keijser *et al.*, 1982), or using more sophisticated Fourier analysis (Delhez *et al.*, 1982; Snyder *et al.*, 1999; Mittemeijer & Scardi, 2003).

It is shown in many textbooks on crystallography that small crystallite size causes a constant broadening of the reciprocal-lattice points, which is a consequence of the Fourier transformation applied to a limited volume (see *e.g.* Giacovazzo *et al.*, 1992). This relationship is well known as the Scherrer formula. Principal work in size analysis has been performed mainly by Langford, Wilson, Louër and Scardi (Langford & Wilson, 1978; Langford & Louër, 1982; Vargas *et al.*, 1983; Langford *et al.*, 2000; Scardi & Leoni, 2001; Popa & Balzar, 2002). On the other hand, the structure defects, which are related to a spatially inhomogeneous change of the interplanar spacing, are responsible for a broadening of the reciprocal-lattice points that increases with the increasing size of the diffraction vector, as can easily be proven by differentiating the Bragg equation. The strain broadening is interpreted either in terms of phenomenological microstrain (Warren, 1990) or in terms of the density of lattice defects, mainly dislocations. The latter approach has been developed mainly

by Wilkens (1970, 1976), Klimanek and Kužel (Klimanek & Kužel, 1988; Kužel & Klimanek, 1988, 1989) and Groma *et al.* (1988). Towards a more general approach, some effort has been made by van Berkum *et al.* (1996), who introduced a model of general defects characterized by a strain field and a distribution of the defects, and by Breuer *et al.* (2000), who suggested a method for separation of the effects related to the so-called second-kind stresses from those related to dislocations.

In recent years, the approach of total-pattern fitting has become popular. Many Rietveld-type routines contain a parameterized description of the size and strain effects (see *e.g.* Rodriguez-Carvajal *et al.*, 1991; Rodriguez-Carvajal, 1993; Balzar *et al.*, 1998; Bergmann *et al.*, 2000; Bergmann & Kleeberg, 2001). An advanced approach consists of a description of the sample microstructure by a model with few free parameters. At least two parameters are related to the effect of size broadening: usually the mean value of the size distribution and its variance. Another two parameters describe the strain broadening: the defect density and the defect correlation, for instance. The first work in this direction was done by Houska and co-workers (Adler & Houska, 1979; Houska & Smith, 1981) in terms of a phenomenological model. A wholly microstructural approach has been developed by the groups of Ungár (Ungár *et al.*, 2001) and Scardi (Scardi & Leoni, 2002). They described the size broadening in a sufficiently general manner (Scardi & Leoni, 2001), whilst the strain broadening was characterized through the dislocation-induced effects according to the Krivoglaz theory (Krivoglaz, 1996) considering the modifications made by Wilkens (1970, 1976) and van Berkum *et al.* (1996).

Since polycrystalline materials with crystallite sizes in the micrometre and sub-micrometre range are most frequently the subject of diffraction studies, the theoretical approaches describing the diffraction phenomena are focused predominantly on the structural defects in the interior of the crystallites. The coherence of X-rays diffracted by different crystallites within a polycrystalline sample is usually neglected, because the large crystallites (micrometre to sub-micrometre) are non-coherent unless they possess extremely strong preferred orientation. A very strong preferred orientation of crystallites improves their mutual coherence, which is observed as secondary extinction (Zachariasen, 1967). The opposite phenomenon, reducing the coherence of the neighbouring crystallites, is a limited coherence length of the radiation, which is approximately 1 μm for conventional diffraction geometry (Černanský, 1982; Holý *et al.*, 1999).

With decreasing crystallite size, the number of imperfections at the crystallite boundaries becomes comparable with the number of internal structural defects. Finally, the structure defects located on the crystallite boundaries become dominant in nanocrystalline materials. Thus, in nanocrystalline materials, the size effect should be dominant; the line broadening should be large and independent of the size of the diffraction vector. This is a result of the kinematical diffraction theory, in which no interference of X-rays scattered by neighbouring crystallites is assumed. However, an increase of the diffraction line broadening with increasing size of the diffraction vector has been observed in nanocrystalline powders (Veprek *et al.*, 1987; Roth *et al.*, 2002) and in nanocrystalline thin films (Rafaja *et al.*, 2004). Veprek and co-workers explained the increasing diffraction line broadening in nanocrystalline powders by variable interplanar spacing across the crystallites. The interplanar spacing was assumed to increase from the centre of the crystallites to the crystallite boundaries as a consequence of the relaxation of interatomic forces at the surface of the crystallites.

Nanocrystallites in the volume of thin films have no free surface; thus we can disregard the relaxation of interatomic forces at the surface of crystallites as an origin of the variations in the interplanar spacing. To be able to explain our recent experimental results (Rafaja *et al.*, 2004) showing apparently a huge inhomogeneous variation of interplanar spacing (large microstrain), we assumed that X-rays scattered by adjacent nanocrystallites are coherent; thus they are capable of interference. The theoretical approach is described in the following sections. Theoretical results were supported by a combination of X-ray diffraction and high-resolution transmission electron microscopy.

2. X-ray diffraction on nanocrystalline domains

The amplitude of X-rays scattered by a nanocrystalline domain is proportional to the structure factor

$$F = \int_V \rho(\mathbf{r}) \exp(i\mathbf{q}\cdot\mathbf{r})\,\mathrm{d}\mathbf{r}, \qquad (1)$$

where $\mathbf{q}$ is the diffraction vector,

$$|\mathbf{q}| \equiv q = (4\pi/\lambda)\sin\theta, \qquad (2)$$

and $\rho(\mathbf{r})$ is the electron density expressed as a function of the position vector $\mathbf{r}$. In equation (2), λ is the wavelength of the radiation and θ is the Bragg angle. The integration in equation (1) is performed over the volume of the crystallite. Alternatively, the shape of a single nanocrystallite can be taken into account by multiplying the electron density with a shape function Ω, which is equal to unity within the crystallite and zero outside:

$$F = \int_{-\infty}^{\infty} \rho(\mathbf{r}) \exp(i\mathbf{q}\cdot\mathbf{r})\Omega(\mathbf{r})\,\mathrm{d}\mathbf{r}. \qquad (3)$$

This corresponds to a convolution of the structure factor calculated for an infinite three-dimensional lattice, F_∞, with the Fourier transform of the shape function, $\mathrm{FT}[\Omega(\mathbf{r})]$:

$$F = F_\infty * \mathrm{FT}[\Omega(\mathbf{r})] = F_\infty * \int_V \exp(i\mathbf{q}\cdot\mathbf{r})\,\mathrm{d}\mathbf{r}. \qquad (4)$$

For spherical crystallites, the Fourier transformation of the shape function has the form

$$\mathrm{FT}[\Omega(\mathbf{r})] = \frac{4\pi}{(\Delta q)^2}\left[\frac{\sin(\Delta q D)}{\Delta q} - D\cos(\Delta q D)\right]. \qquad (5)$$

In equation (5), D denotes the size of the nanocrystalline domain along the diffraction vector and Δq the displacement of the diffraction vector from each reciprocal-lattice point. The structure factor F_∞ is non-zero only in the reciprocal-lattice points. Thus, the convolution yields a constant broadening of the reciprocal-lattice points due to small crystallites. For spherical crystallites, the line broadening is spherically symmetrical in the reciprocal space: it is a spherically symmetrical function of the distance from the respective reciprocal-lattice point, Δq; see equation (5). A rotation of the crystallite corresponds to a rotation of the reciprocal lattice around its origin; a shift of the crystallite corresponds to a change of the phase of the structure factor in equation (4).

3. Relationship between preferred orientation of nanocrystalline domains and their coherence for X-rays

Within the kinematical approach, the diffracted intensity is proportional to the modulus of the structure factor. For two crystallites with the structure factors F_1 and F_1 we obtain

$$I \propto |F_1 + F_2|^2 = |F_1|^2 + 2\Re(F_1^* F_2) + |F_2|^2. \tag{6}$$

Consequently, the waves scattered by two crystallites are coherent (capable of interference) if the interference term is non-zero, which means that the reciprocal-lattice points related to the individual crystallites [equation (5)] overlap each other. Upon this requirement, we can calculate the maximum rotation of two coherent nanocrystalline domains as a function of the crystallite size D. In the first approximation, the maximum rotation ω follows from the geometrical relation (Fig. 1):

$$\omega = 2\arctan(B/2q) = 2\arctan(1/2qD), \tag{7}$$

where B is the intrinsic broadening of an individual reciprocal-lattice point and q the size of the corresponding diffraction vector [equation (2)]. In nanocrystalline materials with a preferred orientation, the adjacent crystallites are coherent with the probability w, which is given by the angular width of the reciprocal-lattice points, ω, and by the width of the texture function G:

$$w = \min\left(\frac{\omega}{G}, 1\right) = \min\left\{\frac{2\arctan[B/(2q)]}{G}, 1\right\}$$
$$\simeq \min\left[\frac{1-(12q^2D^2)^{-1}}{qGD}, 1\right]. \tag{8}$$

The probability w is proportional to the number of coherent crystallites M, which determines, together with the true crystallite size D, the observed line broadening β:

$$\beta \simeq \frac{1}{MD} \propto \frac{1}{wD} \simeq \frac{qG}{1-(12q^2D^2)^{-1}}. \tag{9}$$

For large diffraction vectors $[q > (3.5D)^{-1}]$, equation (9) yields approximately a linear dependence of the observed line broadening on the size of the diffraction vector, which is typical for structures with fluctuations of the interplanar spacing, *i.e.* with microstrain. The slope of the linear dependence depends on the width of the texture function. Strong texture or small crystallites increase the number of coherent crystallites and, consequently, the apparent microstrain. Considering a small crystallite size in nanocrystalline thin films, the limited coherence length of X-rays is not the limiting factor for the coherence of the adjacent crystallites.

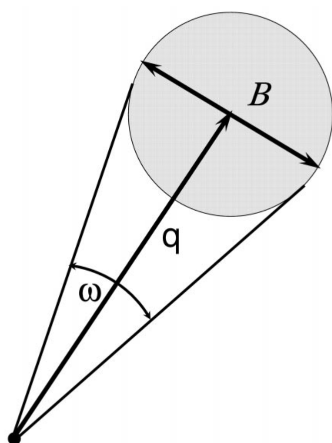

Figure 1
Angular width of a reciprocal-lattice point, ω, as a function of the reciprocal point size, B, and the size of the diffraction vector, q.

4. Interference effects from coherent nanocrystallites

The rigorous description of scattering phenomena in an ensemble of partly coherent nanocrystallites is based on the kinematical formula

$$I \propto |F|^2 \left\langle \sum_n \exp(i\mathbf{q}\cdot\mathbf{R}_n) \cdot \sum_n \exp(-i\mathbf{q}\cdot\mathbf{R}_n) \right\rangle, \tag{10}$$

where F is the structure factor of individual nanocrystalline domains [equation (3)] having the positions $\mathbf{R}_n$. The summation in equation (10) is performed over all crystallites in the irradiated volume, taking into account both the phase shift due to the mutual shift of crystallites and the loss of the coherence due to their rotation. A straightforward calculation (see *e.g.* Rafaja *et al.*, 2000) yields

$$I \propto |F|^2 \left[N + 2\sum_{m=1}^{N-1} w_m (N-m) \Re\langle \exp(i\mathbf{q}\cdot\mathbf{\Delta}_m)\rangle \right]. \tag{11}$$

In equation (11), N denotes the total number of crystallites within the irradiated volume and $\mathbf{\Delta}_m = \mathbf{R}_n - \mathbf{R}_{n+m}$ is the vector connecting two neighbours of the order m. w_m is a weighting factor, which describes the degree of the coherence of the mth neighbours. For coherent crystallites, $w_m = 1$; for incoherent crystallites, $w_m = 0$. It follows from the discussion in the previous section (§3) that the factor w_m depends on the size of the diffraction vector, on the degree of the preferred orientation of crystallites and on the crystallite size. For crystallites with the size and distance D, the projection of the vector $\mathbf{\Delta}_m$ into the direction of the diffraction vector is given by

$$\mathbf{q} \cdot \boldsymbol{\Delta}_m = mqD\cos\alpha, \tag{12}$$

where α is the angle between the vectors $\mathbf{q}$ and $\boldsymbol{\Delta}_m$. Thus, the intensity from equation (11) can be rewritten in the form

$$I \propto |F|^2 \left[N + 2 \sum_{m=1}^{N-1} w_m (N-m) \Re \langle \exp(imqD\cos\alpha) \rangle \right]. \tag{13}$$

The exponential function in equation (13) is averaged over α and D. If the crystallites are randomly distributed around a centre, this averaging yields

$$I \propto N|F|^2 \left[1 + 2 \sum_{m=1}^{N-1} w_m \frac{N-m}{N} \langle J_0(mqD) \rangle \right]. \tag{14}$$

J_0 is the Bessel function, which must be averaged over the inter-crystalline distances D if they are not identical (for a variable crystallite size). Equation (14) is analogous to equation (6), which was used to describe the total intensity diffracted by two coherent crystallites. In equation (14), the term $N|F|^2$ describes the scattering on individual crystallites; the sum represents the interference term. The total intensity can also be understood as a product of the intensity diffracted by individual nanocrystallites with an interference factor (the term in the square brackets), which describes the coherence effects between neighbouring crystallites. If the neighbouring crystallites are not coherent as anticipated in the kinematical diffraction theory, all coefficients w_m are equal to zero. Thus, the total diffracted intensity is given by the sum of the intensity contributions from individual crystallites.

5. Numerical simulation

For partly coherent neighbouring crystallites, w_m is non-zero for small q and small m (neighbouring crystallites). For large m, w_m tends to zero as a result of the limited coherence length of the radiation. For large q, w_m also tends to zero because of the dependence of the angular width of reciprocal-lattice points on the size of the diffraction vector [equation (7)]. The dependence of the weighting factor on the size of the diffraction vector is described by equation (8). The width of the angular distribution of crystallites, G, which is proportional to the width of the texture function, and the line broadening B, which is equal to the true reciprocal crystallite size, are two parameters influencing the weighting factor. The turning point of the weighting factor (Fig. 2*a*) is shifted to larger diffraction vectors either for small crystallites or for strong texture. The interference factor from equation (13) or (14) with w_m from equation (8), is an oscillating function with diminishing amplitudes at large diffraction vectors (Fig. 2*b*). The position of the turning point matches the position of the turning point of the weighting factor. In nanocrystalline materials with partially coherent crystallites, diffraction lines at small diffraction vectors become narrower because of the multiplication of a 'broad' structure factor $N|F|^2$ with a narrow interference factor. For large diffraction vectors, the modulus of the structure factor is multiplied by a constant (the part of the interference factor with shallow oscillations), which does not change the width of diffraction maxima calculated for individual nanocrystallites using equation (5). If N is large and if the weighting factor w_m becomes zero for distant neighbours ($m > 1$), equation (13) yields the following interference factor Φ:

$$\begin{aligned} \Phi &= 1 + \frac{2}{N} \sum_{m=1}^{N-1} w_m (N-m) \Re \langle \exp(imqD\cos\alpha) \rangle \\ &\simeq 1 + w_1 \Re \langle \exp(imqD\cos\alpha) \rangle. \end{aligned} \tag{15}$$

This approximation (only the neighbouring crystallites are coherent) was used for the numerical simulation of the interference factor shown in Fig. 2(*b*). The degree of the preferred orientation of crystallites influences not only the weighting factor [see equation (8)], but also the range of angles α in which the exponential function in equation (15) is averaged.

To be able to compare the results of the numerical simulation with experimental data, a quantity is needed that can be obtained from the experiment: the line width, for instance. The influence of the coherence of adjacent crystallites on the line width can easily be estimated if both the line broadening due to the small crystallite size and the particular oscillations of the interference factor are Gaussian in form. Then the total

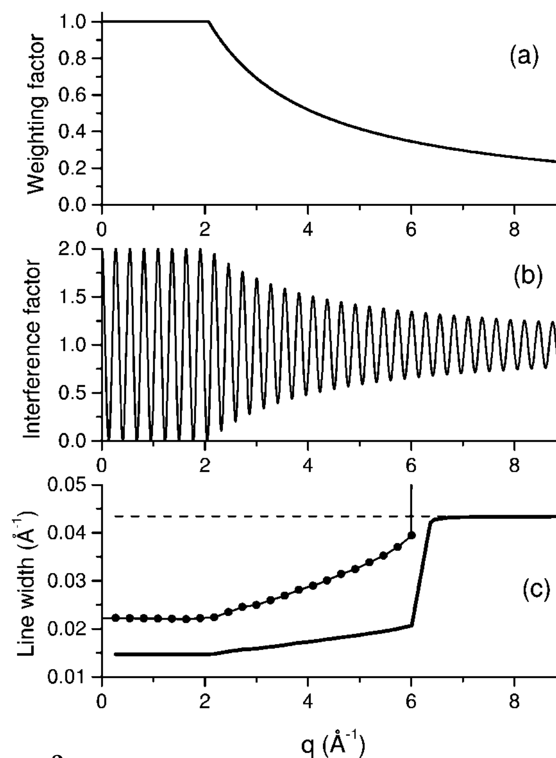

Figure 2
Weighting factor (*a*), interference factor (*b*) and the simulated line width (*c*) as functions of the size of the diffraction vector. In figure (*c*), the line width corresponding to the true crystallite size is plotted by the dashed line; the FWHM of the oscillations of the interference factor are plotted by interconnected circles and the total line width by the solid line. The simulation was performed for the crystallite size D = 2.4 nm and for G = 2.4°.

line width (Fig. 2*c*) is given by the geometrical mean of the individual broadenings B and β:

$$\beta_{\text{total}} = B\beta/(B + \beta). \tag{16}$$

The line broadening due to the small crystallite size, B, is constant. The contribution of the interference factor to the line width, β, can be divided into three regions. For small diffraction vectors, where the adjacent crystallites are entirely coherent (*i.e.* the weighting factor is equal to unity), the width of the oscillations of the interference factor is independent of the diffraction vector and small with respect to the line broadening due to small crystallites. Thus, the total line broadening is determined mainly by the width of the oscillations of the interference factor; the influence of the true size effect is negligible as a result of the geometrical average in equation (16). For intermediate diffraction vectors, the adjacent crystallites are only partially coherent. Thus the oscillations of the interference factor become shallower and the 'sharpening' of diffraction lines due to the coherence of adjacent crystallites is less pronounced. This effect results in an increase of the total line broadening with increasing size of the diffraction vector. When the amplitudes of the interference factor have dropped below half of the maximum intensity, the effect of the coherence of the neighbouring crystallites on the total line broadening becomes negligible. For such diffraction vectors, the total line broadening is given by diffraction effects on small mutually incoherent crystallites, and therefore it is independent of the size of the diffraction vector. The increase of the line broadening with increasing diffraction vector in the intermediate range can falsely be understood as a consequence of the microstrain in the sample. Besides, the increase of the line broadening can change the crystallite size as calculated from the extrapolation of the line broadening to $q = 0$.

Although the diffraction line broadening is influenced by the partial coherence of adjacent crystallites, the dependence of the total line broadening on the size of the diffraction vector discussed above can be exploited to determine the correct crystallite size in nanocrystalline samples. The line breadth that is observed at large diffraction angles (large q) reveals true diffraction line broadening due to the size effect (and microstrain, if any) within individual (mutually incoherent) nanocrystallites. The line broadening at low diffraction angles (small q) can be additionally influenced by the structural defects located at the crystallite boundaries, which become visible because of the partial coherence of adjacent crystallites. The position of the transition zone, where the line broadening increases steeply, depends on the true crystallite size and on the degree of the preferred orientation of crystallites. These two parameters are the only free parameters of the microstructural model. Fig. 3 shows the influence of the parameters on the shape of the interference factor. For larger crystallites, the transition zone is shifted to smaller diffraction vectors; the same is true for the region of the diffraction angles, where the measured line broadening is uninfluenced by the partial coherence of crystallites. The effect of the preferred orientation of crystallites is much more pronounced. Even a crystallite size of 2.4 nm is not sufficient to obtain a mutual coherence if the crystallites are randomly oriented (Fig. 3*c*).

6. Experimental results

The theoretical results were compared with experimental data obtained on nanocrystalline $Ti_{1-x}Al_xN$ (x = 0.62 and 0.04) thin films. These films were prepared by arc evaporation in nitrogen atmosphere with a working pressure of 1.3 Pa using two cathodes made of titanium and aluminium, respectively (Holubář *et al.*, 2000). The ion current on the Al cathode was 120 A; that on titanium was 80 A. Polished plates of sintered tungsten carbide were used as substrates. The bias voltage was −75 V.

The samples were analysed using glancing-angle X-ray diffraction (GAXRD) and high-resolution transmission electron microscopy (HRTEM). The GAXRD experiments were performed at the beamline B2 at HASYLAB/DESY at the wavelength of 1.1314 Å, which was selected by a germanium (111) double monochromator and verified by a measurement on a polycrystalline silicon standard. The diffraction measurements on the thin films were made at a constant angle of incidence (2°); this angle was chosen to reduce the penetration depth of the radiation into the sample. A good angular resolution in the diffracted beam was guaranteed by a flat perfect (111)-oriented germanium single-crystal analyser, located in the front of a scintillation detector. In this experimental setup, the instrumental line broadening (FWHM) is

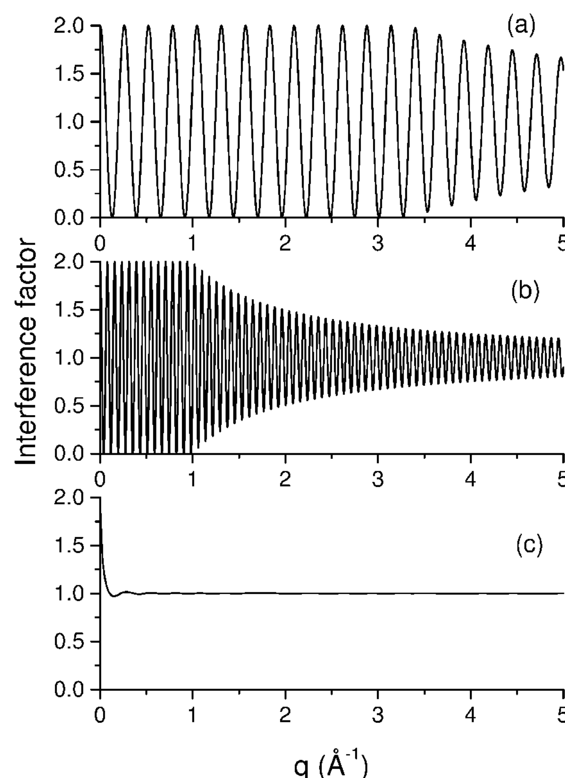

Figure 3
The interference factor simulated for different crystallite sizes and textures. (*a*) D = 2.4 nm, G = 1.5°; (*b*) D = 8.0 nm, G = 1.5°; (*c*) D = 2.4 nm, no texture.

below 0.01° as measured with the LaB_6 standard from NIST; thus the instrumental line broadening was neglected. HRTEM was performed using the 200 kV analytical high-resolution transmission electron microscope JEM 2010 FEF with an ultra-high resolution objective lens (C_s = 0.5 mm) and an in-column energy filter to select only the elastic electrons for the image recording. The specimens were prepared with so-called plane view orientation. After a mechanical pre-thinning, the specimens for HRTEM were etched by an ion beam. The final step in the specimen preparation was the plasma cleaning procedure. These experiments were completed by X-ray texture analysis, which was performed on a laboratory source (copper anode, λ = 1.5418 Å) with a powder diffractometer equipped by an Eulerian cradle.

In the sample with the chemical composition $Ti_{0.38}Al_{0.62}N$ (determined by electron probe microanalysis with wavelength-dispersive X-ray spectroscopy), HRTEM imaging (Fig. 4) revealed the nanocrystalline structure in the total electron-transparent region. The crystallite size was obtained from the size of domains with a good long-range periodicity of the electron density, as investigated *via* line scans drawn in the HRTEM image along crystallographic directions with low indices, such as the line scan along [100] shown in Fig. 5. The continuous regions with a good periodicity of the electron density were assigned to individual crystallites. A mean crystallite size of approximately 3.5 nm was determined. The crystallite size that was calculated from the line broadening measured at high diffraction angles using GAXRD was 2.4 nm. The simulated line broadening performed with this crystallite size and with G = 2.4° matches well the experimental data (Fig. 6). The high preferred orientation of crystallites in this sample was confirmed by a detailed texture analysis. The component method (Helming *et al.*, 1994) applied to the pole figures measured on the diffraction lines 111, 200 and 220 (Fig. 7) has shown that the dominant texture component has a half-width of 31°.

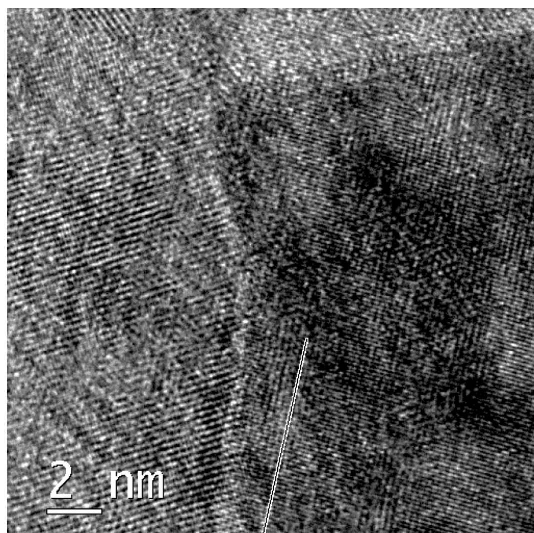

Figure 4
HRTEM image of the nanocrystalline $Ti_{0.38}Al_{0.62}N$ thin film.

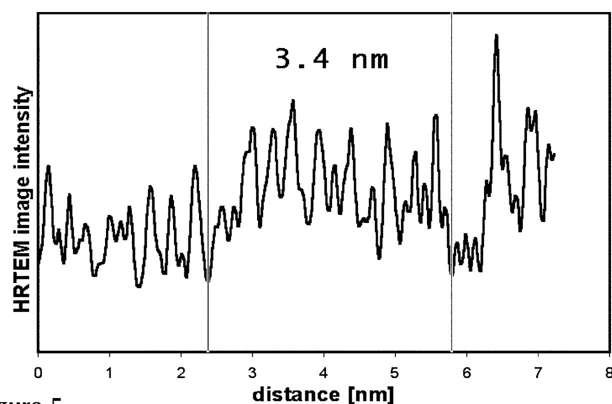

Figure 5
An example of the line scan (taken along the line in Fig. 4) showing the variations in the electron density. The good periodicity of the electron density in the middle range of the scan is related to the long-range periodicity of the crystal structure (here in the direction [111]). The size of the domains with a good long-range periodicity defines the crystallite size.

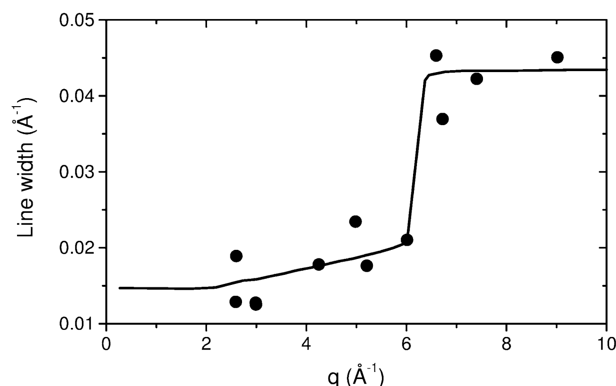

Figure 6
Diffraction line broadening measured for the nanocrystalline $Ti_{0.38}Al_{0.62}N$ thin film (points) and the numerical simulation (solid line).

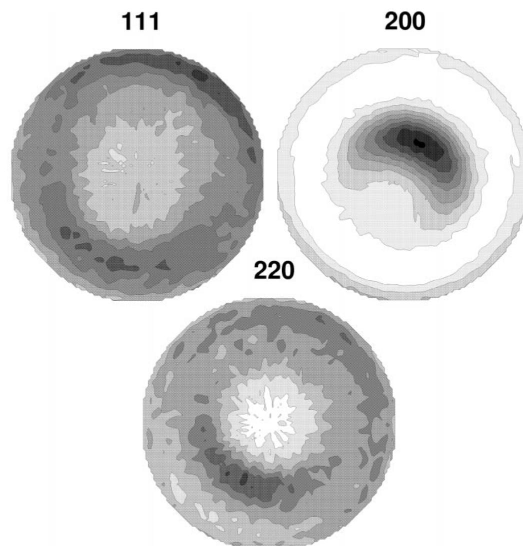

Figure 7
Pole figures recorded for the diffraction lines 111, 200 and 220 of the nanocrystalline thin film $Ti_{0.38}Al_{0.62}N$.

A similar dependence of the line width on the size of the diffraction vector was observed in another thin film with the chemical composition $Ti_{0.96}Al_{0.04}N$ (Fig. 8). The maximum line broadening measured at high diffraction angles yielded the true crystallite size of 8.0 nm. Although this sample has approximately two times stronger preferred orientation of crystallites than the previous one (the half-width of the dominant texture component obtained using the component method was 14°), the steep increase of the line width is shifted to smaller diffraction vectors. This is a consequence of the faster decrease of the weighting factor for larger crystallites, as discussed in previous sections. The pole figures recorded for the diffraction lines 111, 200 and 220 are shown in Fig. 9. The parameter G = 1.5° yielded the best match between the experimental and the simulated data. A smaller value of the parameter G corresponds to a stronger preferred orientation of crystallites.

7. Discussion

The theoretical results used for the numerical simulation were obtained under the assumption that only the adjacent crystallites can be coherent. Another approximation was applied when the individual oscillations of the interference factor were described by Gaussian functions. These approximations have no influence on the true crystallite size calculated from the diffraction line broadening at high diffraction angles, because this diffraction line broadening is unaffected by the coherence of the adjacent crystallites. On the other hand, the approximations have a serious influence on the parameter G calculated from the position of the steep increase of the diffraction line broadening with increasing size of the diffraction vector. This means that the value of the parameter G does not have to match numerically the width of the texture function obtained from the texture analysis, as confirmed by the experimental data. Nevertheless, a stronger preferred orientation of crystallites (a smaller width of the texture function) was accompanied by a decrease of the parameter G in the microstructure model.

Despite the approximations, this theoretical consideration explained quite well the dependence of the diffraction line broadening on the size of the diffraction vector, which is often observed in nanocrystalline materials: a steep increase of the diffraction line broadening with increasing size of the diffraction vector at low diffraction angles and a constant line broadening at high diffraction angles. With increasing crystallite size or with decreasing preferred orientation of crystallites, the turning point of the dependence β *versus* q is shifted to lower diffraction angles. In samples with large crystallites, the oscillations of the interference factor and a consequent 'sharpening' of the diffraction lines could only be observed at extremely small scattering angles in small-angle X-ray scattering (Guinier & Fournet, 1955; Glatter & Kratky, 1982). The diffraction line broadening observed in large crystallites at usual diffraction angles is uninfluenced by the partial coherence of adjacent crystallites, as known from the kinematical diffraction theory.

Synchrotron radiation was used because it offers several advantages. It is highly coherent at a high intensity of the primary beam; the high intensity improves the statistical quality of experimental data considerably. The coherence length of the synchrotron radiation can be regarded as infinite compared with the size of the crystallites. High coherence of radiation in the primary and diffracted beam implies negligible instrumental line broadening. However, the instrumental broadening of diffraction lines is also negligible if nanocrystalline materials are investigated on a conventional diffractometer, as seen by comparison of the synchrotron data with the laboratory data. The diffraction line breadths measured with synchrotron and laboratory sources were principally identical, but the precision of the laboratory data is much lower because of the low intensity of the radiation. The short wavelength used for the measurements makes the accessible

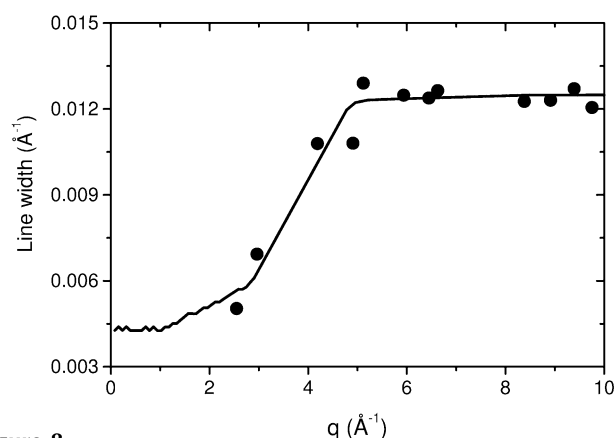

Figure 8
Diffraction line broadening measured for the nanocrystalline $Ti_{0.96}Al_{0.04}N$ thin film (points) and the numerical simulation (solid line). The scatter of the calculated curve at small scattering vectors is due to numerical errors.

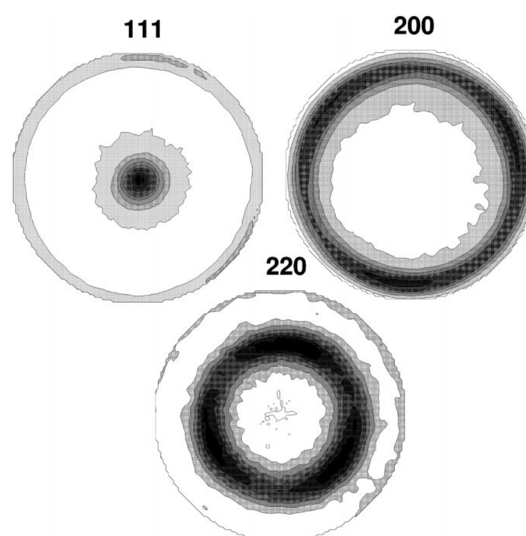

Figure 9
Pole figures recorded for the diffraction lines 111, 200 and 220 of the nanocrystalline thin film $Ti_{0.96}Al_{0.04}N$.

range of the diffraction vectors broader: the diffraction pattern contained more diffraction lines.

8. Conclusions

The partial coherence of adjacent nanocrystallites can be understood as an overlap of the respective reciprocal-lattice points. It was concluded from theoretical considerations that small size and strong preferred orientation of crystallites improve their coherence. The small crystallite size causes an overall broadening of the reciprocal-lattice points; the strong texture reduces the mutual rotations of the reciprocal lattices belonging to individual crystallites. Both phenomena enhance the overlap of the reciprocal-lattice points related to the coherence of adjacent crystallites. Because the angular width of the reciprocal-lattice points (as related to the rotation of the reciprocal lattice around its origin) decreases with increasing size of the diffraction vector, the coherence effects are suppressed with increasing diffraction angle. The coherence of adjacent crystallites reduces the diffraction line broadening at low diffraction angles. On the other hand, an increase of the diffraction line broadening can be anticipated at higher diffraction angles, where the coherence of the adjacent crystallites becomes extinct. The increase of the diffraction line broadening with increasing diffraction angle observed in the intermediate range of the diffraction angles can be misinterpreted as microstrain. Furthermore, the partial coherence of the adjacent nanocrystallites can influence the crystallite size calculated from the extrapolation of the line broadening to the origin of the reciprocal space. These theoretical results were confirmed by experimental data obtained on nanocrystalline thin films of titanium aluminium nitrides using a combination of glancing-angle X-ray diffraction and high-resolution transmission electron microscopy. The diffraction line broadening observed in X-ray diffraction experiments was fitted by using a theoretical model having two free parameters: the true crystallite size and the degree of the preferred orientation of crystallites. The small crystallite size calculated using this model was confirmed by high-resolution transmission electron microscopy; the high degree of preferred orientation of crystallites was confirmed by texture analysis.

The HRTEM JEM 2010 FEF was financed through Deutsche Forschungsgemeinschaft in the frame of the Priority Program #1062. The financial support from the Grant Agency of the Czech Republic (project #106/03/0819) is also acknowledged. The synchrotron measurements at the beamline B2 at HASYLAB/DESY were supported by the BMBF Project #05KS1RDA/9. The samples of the nanocrystalline thin films of titanium aluminium nitride were provided by Dr M. Šima of the SHM Company (Nový Malín, Czech Republic).

References

Adler, T. & Houska, C. R. (1979). *J. Appl. Phys.* **50**, 3282–3287.
Balzar, D., Von Dreele, R. B., Bennett, K. & Ledbetter, H. (1998). *J. Appl. Phys.* **84**, 4822–4833.
Bergmann, J., Kleeberg, R., Haase, A. & Breidenstein, B. (2000). *Mater. Sci. Forum*, **347**, 303–308.
Bergmann, J. & Kleeberg, R. (2001). *Mater. Sci. Forum*, **378**, 30–35.
Berkum, J. G. M. van, Delhez, R., de Keijser, Th. H. & Mittemeijer, E. J. (1996). *Acta Cryst.* A**52**, 730–747.
Breuer, D., Klimanek, P. & Pantleon, W. (2000). *J. Appl. Cryst.* **33**, 1284–1294.
Čerňanský, M. (1982). *Phys. Status Solidi B*, **114**, 365–372.
Delhez, R., de Keijser, Th. H. & Mittemeijer, E. J. (1982). *Z. Anal. Chem.* **312**, 1–16.
Giacovazzo, C., Monaco, H. L., Viterbo, D., Scordari, F., Gilli, G., Zanotti, G. & Catti, M. (1992). *Fundamentals of Crystallography*. IUCr/Oxford University Press.
Glatter, O. & Kratky O. (1982). *Small-Angle X-ray Scattering*. London: Academic Press.
Groma, I., Ungár, T. & Wilkens, M. (1988). *J. Appl. Cryst.* **21**, 47–53.
Guinier, A. & Fournet, G. (1955). *Small-Angle Scattering of X-rays*. New York: John Wiley.
Helming, K., Schwarzer, R. A., Rauschenbach, B., Geier, S., Leiss, B., Wenk, H. R., Ullemeyer, K. & Heinitz, J. (1994). *Z. Metallkunde*, **85**, 545–553.
Holubář, P., Jílek, M. & Šima, M. (2000). *Surf. Coat. Technol.* **133**, 145–151.
Holý, V., Pietsch, U. & Baumbach, T. (1999). *High-Resolution X-ray Scattering from Thin Films and Multilayers, Springer Tracts in Modern Physics 149*. Berlin: Springer-Verlag.
Houska, C. R. & Smith, T. M. (1981). *J. Appl. Phys.* **52**, 748–753.
Keijser, Th. H. de, Langford, J. I., Mittemeijer, E. J. & Vogels, A. B. P. (1982). *J. Appl. Cryst.* **15**, 308–313.
Klimanek, P. & Kužel, R. (1988). *J. Appl. Cryst.* **21**, 59–66.
Krivoglaz, M. A. (1996). *X-ray and Neutron Diffraction in Non-ideal Crystals*. Berlin: Springer-Verlag.
Kužel, R. & Klimanek, P. (1988). *J. Appl. Cryst.* **21**, 363–368.
Kužel, R. & Klimanek, P. (1989). *J. Appl. Cryst.* **22**, 299–307.
Langford, J. I. & Louër, D. (1982). *J. Appl. Cryst.* **15**, 20–26.
Langford, J. I., Louër, D. & Scardi, P. (2000). *J. Appl. Cryst.* **33**, 964–974.
Langford, J. I. & Wilson, A. J. C. (1978). *J. Appl. Cryst.* **11**, 102–113.
Mittemeijer, E. J. & Scardi, P. (2003). *Diffraction Analysis of the Microstructure of Materials*. Berlin: Springer-Verlag.
Popa, N. C. & Balzar, D. (2002). *J. Appl. Cryst.* **35**, 338–346.
Rafaja, D., Šima, M., Klemm, V., Schreiber, G., Heger, D., Havela, L. & Kužel, R. (2004). *J. Alloys Compd.* In the press.
Rafaja, D., Valvoda, V., Kub, J., Temst, K., Van Bael, M. J. & Bruynseraede, Y. (2000). *Phys. Rev. B*, **61**, 16144–16153.
Rodriguez-Carvajal, J. (1993). *Physica B*, **192**, 55–69.
Rodriguez-Carvajal, J., Fernandez-Diaz, M. T. & Martinez, J. L. (1991). *J. Phys. Condens. Matter*, **3**, 3215–3234.
Roth, C., Martz, N., Hahn, F., Leger, J. M., Lamy, C. & Fuess, H. (2002). *J. Electrochem. Soc.* **149**, E433–E439.
Scardi, P. & Leoni, M. (2001). *Acta Cryst.* A**57**, 604–613.
Scardi, P. & Leoni, M. (2002). *Acta Cryst.* A**58**, 190–200.
Snyder, R. L., Fiala, J. & Bunge, H. J. (1999). *Defect and Microstructure Analysis by Diffraction*. Oxford University Press.
Ungár, T., Gubicza, J., Ribárik, G. & Borbély, A. (2001). *J. Appl. Cryst.* **34**, 298–310.
Vargas, R., Louër, D. & Langford, J. I. (1983). *J. Appl. Cryst.* **16**, 512–518.
Veprek, S., Sarott, F. A. & Iqbal, Z. (1987). *Phys. Rev. B*, **36**, 3344–3350.
Warren, B. E. (1990). *X-ray Diffraction*. New York: Dover.
Wilkens, M. (1970). *Phys. Status Solidi A*, **2**, 359–370.
Wilkens, M. (1976). *Krist. Technik*, **11**, 1159–1169.
Williamson, G. K. & Hall, A. H. (1953). *Acta Metall. Mater.* **1**, 22–31.
Zachariasen, W. H. (1967). *Acta Cryst.* **23**, 558.